New Astronomy 38 (2015) 16–22

Contents lists available at ScienceDirect

New Astronomy

journal homepage: www.elsevier.com/locate/newast

Photoionization of ground and excited states of Ti I

Sultana N. Nahar *

Department of Astronomy, The Ohio State University, Columbus, OH 43210, United States

HIGHLIGHTS

- Photoionization of Ti I for the ground and many excited states is studied with details for the first time.
- Study reveals dominant resonant features at low energy that will affect plasma opacity.
- Highly excited states also show enhanced Seaton resonances.
- All features will have significant contributions to both photoionization and recombination rates.
- These should provide more precise determination of abundances and diagnostics of cool and red giant stars.

ARTICLE INFO

Article history:
Received 3 September 2014
Received in revised form 25 December 2014
Accepted 7 January 2015
Available online 20 January 2015
Communicated by G.F. Gilmore

Keywords:
Photoionization of Ti I
Cross sections of excited levels
R-matrix method
Resonant features

ABSTRACT

Detailed photoionization of ground and many excited states with autoionizing resonances of neutral Ti are presented. Ti I with 22 electrons forms a large number of bound states, the present work finds a total of 908 bound states with $n \leqslant 10$ and $l \leqslant 8$. Photoionization cross sections (σ_{PI}) for all these bound states have been obtained. Calculations were carried out in the close-coupling R-matrix method using a wave function expansion that included 36 states of core ion Ti II. It is found that the resonances enhance the low energy region of photoionization of the ground and low lying excited states. The resonant features will increase the opacity, as expected of astrophysical observation, and hence play important role in determination of abundances in the elements in the astronomical objects. The excited states also show prominent structures of Seaton or photo-excitation-of-core resonances.

1. Introduction

Ti I is commonly seen in the spectra of red giant stars (RGS), the dying stars near the end of stellar evolution, and of cool M stars (e.g. Keenan, 1982, 1998). Photoionized Ti I is locked to TiO which causes opacity or flux absorption distribution of the outer layers. Abundance of TiO molecule can have crucial and measurable consequences on the atmospheric structure and spectra of cool stars. The vibrational bands of TiO are used as temperature indicators for these stars. stellar parameters and abundances for RGS stars. The spectral analysis, modeling of abundances require photoionization cross sections of Ti I. Ti I is also abundant in the spectra of Large Magellanic Cloud, a small satellite galaxy of Milky Way, but is a prime target to probe the chemical evolution of stars (e.g. Wood et al., 2013). The resonances in σ_{PI} can also be seen in absorption spectra. These cross sections are needed for electron–ion recombination, opacity or radiation flux calculations, elemental abundances, ionization fractions, etc.

Limited number of studies were carried out for the radiative process for Ti I. Sohl et al. (1990) and Page and Gudeman (1990) studied high-n, above $n = 14$ and going up to 40, resonances of a few excited core state using two-photon experiment. Sohl et al. also carried out multichannel quantum defect calculations in order to determine accurate ionization potentials. These high lying resonances are narrow and they converge on to various excited core states. Miecznik and Greene (1996) calculated the high-n resonances for three excited levels of Ti I using R-matrix method and quantum defect theory and showed good agreement with the high-n resonances measured by Sohl et al. (1990). These high lying resonances are often well-structured at well-defined energies and less perturbed by the correlation effects. Miecznik and Greene (1996) used a 14-states wave function expansion where as a 36-states expansion is used in the present work. McLaughlin and Duquette (1992) measured photoionization cross sections in a small energy range of excited $3d^2 4s4p(^3P_2)$ level of Ti I.

The present work gives detailed resonances up to $n = 10$ as these provide the most significant contributions. The R-matrix calculations

* Tel.: +1 614 292 1888; fax: +1 614 292 2928.
E-mail address: nahar.1@osu.edu
URL: http://www.astronomy.ohio-state.edu/~nahar

http://dx.doi.org/10.1016/j.newast.2015.01.001
1384-1076/

under the Opacity Project (OP) (The Opacity Project Team, 1995) and the Iron Project (IP) (Hummer et al., 1993), such as the present work, provide averaged values of the high-n narrow resonances by using Gailities averaging procedure (e.g. illustrated in Nahar and Pradhan (1991)). The first systematic study of photoionization of many atoms and ions, abundant in astrophysical plasmas, were carried out under the OP (The Opacity Project Team, 1995) largely for plasma opacity calculations. The follow-up project the Iron Project (Hummer et al., 1993) which focuses both collisional and radiative processes of mainly iron-peak elements, such as Ti I, as mentioned above, the present study is carried out under the IP.

2. Theory and computations

Photoionization of an atomic system with more than one electron show resonant features. The process can occur directly,

$$h\nu + X^{+} \rightarrow e + X^{++}, \tag{1}$$

as well as through an intermediate doubly excited autoionization state

$$e + X^{++} \leftrightharpoons (X^{+})^{**} \leftrightharpoons \begin{cases} (a)\ e + X^{++}(AI) \\ (b)\ h\nu + X^{+}(DR) \end{cases}, \tag{2}$$

where the intermediate doubly excited autoionizing state leads either to autoionization (AI) where the electron goes free or to dielectronic recombination (DR) where the electron is captured by emission of a photon (e.g. Pradhan and Nahar, 2011). An autoionizing state introduce a resonance. Theoretically the doubly excited state is obtained by including the core excitations in the wave function, as considered in close coupling (CC) approximation.

In CC approximation the atomic system is represented by a 'target' or the 'core' ion of N-electrons system interacting with the $(N+1)$ th electron. The $(N+1)$ th electron is bound if the energy E is negative or in the continuum if it is negative. The total wave function, Ψ_E, of the $(N+1)$ electrons system in a symmetry $SL\pi$ is represented by an expansion as

$$\Psi_E(e + ion) = A\sum_i \chi_i(ion)\theta_i + \sum_j c_j \Phi_j, \tag{3}$$

where the target ion eigenfunction, χ_i, is coupled with the $(N+1)$ th electron function, θ_i. The sum is over the ground and excited core states. The $(N+1)$ th electron with kinetic energy k_i^2 is in a channel labeled as $S_iL_i\pi_i k_i^2 \ell_i (SL\pi)$. In the second sum, the Φ_js are bound channel functions of the $(N+1)$-electrons system that account for short range correlation and the orthogonality between the continuum and the bound electron orbitals. Substitution of $\Psi_E(e + ion)$ in the Schrodinger equation

$$H_{N+1}\Psi_E = E\Psi_E \tag{4}$$

introduces a set of coupled equations that are solved using the R-matrix approach. The solution is a continuum wave function, Ψ_F, for an electron with positive energies ($E > 0$), or a bound state, Ψ_B, at a negative total energy ($E \leqslant 0$). The details of the R-matrix method in the CC approximation can be found in, e.g. Burke and Robb (1975), Seaton (1987), Berrington et al. (1987), Pradhan and Nahar (2011). Present calculations are carried out in LS coupling approximation where the Hamiltonian of the $(N+1)$-electrons system is given by

$$H_{N+1} = \sum_{i=1}^{N+1}\left\{-\nabla_i^2 - \frac{2Z}{r_i} + \sum_{j>i}^{N+1}\frac{2}{r_{ij}}\right\}, \tag{5}$$

Transition matrix elements for photoionization, $\langle \Psi_B || \mathbf{D} || \Psi_F \rangle$ where $\mathbf{D} = \sum_i r_i$ is the dipole operator and the sum is over the number of electrons, are obtained from the bound and continuum wave functions. The transition matrix element is reduced to generalized line strength as

$$\mathbf{S} = \left|\langle \Psi_j || \mathbf{D} || \Psi_i \rangle\right|^2 = \left|\left\langle \psi_f \mid \sum_{j=1}^{N+1} r_j \mid \psi_i \right\rangle\right|^2, \tag{6}$$

where Ψ_i and Ψ_f are the initial and final state wave functions. The photoionization cross section (σ_{PI}) is proportional to the generalized line strength,

$$\sigma_{PI} = \frac{4\pi^2}{3c}\frac{1}{g_i}\omega\mathbf{S}, \tag{7}$$

where g is the statistical weight factor of the bound state and ω is the incident photon energy. The details of the R-matrix method in the CC approximation for photoionization can be found in,.e.g. Pradhan and Nahar (2011). The complex resonant structures in photoionization result from couplings between the continuum channels and bound channels in transition matrix at electron energies k_i^2 corresponding to autoionizing states of the Rydberg series, $S_iL_i\pi_i\nu\ell$ where ν is the effective quantum number, belonging to excited target or core state $S_iL_i\pi_i$.

3. Computation

The R-matrix calculation is initiated with the wave function of core ion as the input. For the core ion, Ti II, the wave function was obtained from optimization of atomic structure calculations of the ground and 10 excited configurations, as listed in Table 1, using the later version (Nahar et al., 2003) of atomic structure code SUPERSTRUCTURE (SS) (Eissner et al., 1974). SS uses Thomas–Fermi approximation. Table 1 presents the Thomas–Fermi scaling parameters for the orbitals. The calculated energies are compared with the observed values in the compilation of Saloman (2012) and listed in NIST web site (YYYY, XXXX). The observed energies of fine structure level energies have been statistically averaged to obtain the LS term energies. The comparison is good in general except for a few states where the difference is large. Being near neutral, the wave function is sensitive to set of configurations being used. The target set was optimized for the given configurations with the values of scaling parameters in Table 1. It may be noted that results from a R-matrix calculation are often less sensitive to core energies because of achieving higher accuracy from interaction of a large number of configurations.

The partial wave expansion of the interacting electron includes orbital angular momenta of $0 \leqslant \ell \leqslant 9$, with a R-matrix basis set of 12 continuum functions. The second term of the wave function in Eq. (3), which represents the bound state correlation functions, includes 40 $(N+1)$-particle configurations with orbital occupancies from minimum to a maximum number as given within parentheses of the orbitals 3s(0–2), 3p(4–6), 3d(1–6), 4s(0–2), 4p(0–2), 4d(0–2), 4f(0–1) with filled core shells $1s^2 2s^2 2p^6$ for each configuration. Computations are carried out for all angular momenta, $0 \leqslant L \leqslant 13$ of quintets, triplets and singlets.

All energy eigenvalues were scanned with quantum defect of 0.001. They were identified with spectroscopic designation using quantum defect analysis and percentage of channel contributions to the states with code ELEVID (Nahar, 2006). For resonances in photoionization, σ_{PI}, in the near threshold energy region was resolved with a finer energy mesh, such as, 3000 energy points up to 0.4 Ry above the ionization threshold. The cross section files were processed with code PRCLS.

4. Results and discussions

The present work reports large number of bound states and photoionization cross sections of each of them The results are discussed in separate sections below.

Table 1
Thirty-six LS states and energies (E_t) of core ion Ti II in wave function expansion of Ti I. They were optimized using a set of 11 spectroscopic configurations: $3s^23p^63d^24s(1)$, $3s^23p^63d^3(2)$, $3s^23p^63d^24p(3)$, $3s^23p^63d^24d(4)$, $3s^23p^63d4s4p(5)$, $3s^23p^63d4s^2(6)$, $3s^23p^63d^24f(7)$, $3s^23p^53d^4(8)$, $3s^23p^43d^5(9)$, $3s3p^63d^4(10)$, $3p^63d^5(11)$ with filled $1s^22s^22p^6$ orbitals. The Thomas–Fermi scaling parameters for the orbitals are 1.15(1s), 1.10(2s), 1.10(2p), 1.15(3s), 1.10(3p), 1.10(3d), 1.0(4s), 1.0(4p), 1.0(4d), 1.0(4f). The present calculated energies (SS) are compared with observed energies in NIST compilation.

	State		E_t (Ry) SS	E_t (Ry) NIST
1	$3d2(3F)4s$	a^4F	0.0	0.002052
2	$3d3$	b^4F	0.008475	0.009891
3	$3d2(3F)4s$	a^2F	0.052914	0.043580
4	$3d2(1D)4s$	a^2D	0.096937	0.079561
5	$3d3$	a^2G	0.109467	0.082604
6	$3d3$	a^4P	0.103114	0.086130
7	$3d3$	a^2P	0.188752	0.090528
8	$3d2(3P)4s$	b^4P	0.109190	0.090836
9	$3d32$	b^2D	0.147753	0.115790
10	$3d3$	a^2H	0.162962	0.116008
11	$3d2(1G)4s$	b^2G	0.163011	0.139070
12	$3d2(3P)4s$	b^2P	0.108887	0.151168
13	$3d3$	b^2F	0.250445	0.190614
14	$3d4s2$	c^2D	0.348422	0.228730
15	$3d2(3F)4p$	z^4G^o	0.253728	0.272803
16	$3d2(3F)4p$	z^4F^o	0.264008	0.283475
17	$3d2(3F)4p$	z^2F^o	0.271306	0.285860
18	$3d2(3F)4p$	z^2D^o	0.276977	0.290858
19	$3d2(1S)4s$	a^2S	0.363831	0.289673
20	$3d31$	d^2D	0.425681	0.294430
21	$3d2(3F)4p$	z^4D^o	0.279072	0.297894
22	$3d2(3F)4p$	z^2G^o	0.302906	0.315821
23	$3d2(3P)4p$	z^2S^o	0.342864	0.341094
24	$3d2(1D)4p$	z^2P^o	0.357275	0.358862
25	$3d2(1D)4p$	y^2D^o	0.361207	0.360199
26	$3d2(1D)4p$	y^2F^o	0.362178	0.364610
27	$3d2(3P)4p$	z^4S^o	0.365088	0.364755
28	$3d2(3P)4p$	y^4D^o	0.368311	0.370084
29	$3d2(3P)4p$	z^4P^o	0.382594	0.383888
30	$3d2(1G)4p$	y^2G^o	0.397785	0.398799
31	$3d2(3P)4p$	x^2D^o	0.413399	0.409227
32	$3d2(3P)4p$	y^2P^o	0.420341	0.414840
33	$3d2(1G)4p$	z^2H^o	0.416299	0.417378
34	$3d2(1G)4p$	x^2F^{o*}	0.433495	0.433167
35	$3d(2D)4s4p(3Po)$	$^4F^o$	0.591665	0.480615
36	$3d(2D)4s4p(3Po)$	$^4D^o$	0.595097	0.479818

4.1. LS term energies

A total of 908 bound states with $n \leqslant 10$ and $l \leqslant 8$ of Ti I have been obtained. All states have been identified through quantum defect analysis and percentage channel contributions to the state. A Rydberg series of states can be isolated out from the quantum defect μ, which remains approximately the same, and effective quantum number ν which increases by unity for higher states of the series. The equivalent electron states can be estimated from determination of all states from the possible configurations. For example, with the given target states in Table 1, the possible equivalent electron states will form from $3d^24s^2$, $3d^4$, and $3d^23p^2$ configurations. These states can also be identified by comparing with existing states, such as those found in the NIST table.

The present energies account for all observed states, 159 in total. These LS states were obtained from statistical averaging of observed fine structure levels compiled, as in the case of Ti II, by Saloman (2012) and available in the NIST table (YYYY, XXXX). There are several states whose spectroscopic identifications show some difference with those listed at NIST. For example, identification of state $3d^23P4s4p^3P^o(y^1P^o)$ differs from $3d^23P4s4p(^3P^o)$ in the

Table 2
Comparison of calculated LS term energies, E_c, of Ti I with term energies, E_o, obtained from statistical averaging of energies of observed fine structure levels (YYYY, XXXX). The number next to a LS state symmetry refers its position in the calculated energies of the symmetry.

Conf	Term	E_o (Ry)	E_c (Ry)
$3d^24s^2$	a^3F:1	0.499262	0.5074834
$3d^3(^4F)4s$	a^5F:1	0.440040	0.5005332
$3d^24s^2$	a^1D:1	0.435174	0.4344129
$3d^24s^2$	a^3P:1	0.423401	0.4349205
$3d^3(^4F)4s$	b^3F:2	0.394920	0.4427572
$3d^24s^2$	a^1G:1	0.390859	0.4007668
$3d^3(^4P)4s$	a^5P:1	0.373210	0.4274615
$3d^3(^2G)4s$	a^3G:1	0.363050	0.4090051
$3d^23F4s4p^3P^o$	z^5G^o:1	0.353649	0.3719663
$3d^23F4s4p^3P^o$	z^5F^o:1	0.345957	0.3673404
$3d^3(^2D2)4s$	a^3D:1	0.342116	0.3940433
$3d^3(^2P)4s$	b^3P:2	0.336343	0.3657704
$3d^3(^2H)4s$	a^3H:1	0.336049	0.3712170
$3d^3(^2G)4s$	b^1G:2	0.334641	0.3483942
$3d^23F4s4p^3P^o$	z^5D^o:1	0.331812	0.3491138
$3d^3(^2P)4s$	c^3P:3	0.329311	0.3575310
$3d^23F4s4p^3P^o$	z^3F^o:1	0.323926	0.3329441
$3d^23F4s4p^3P^o$	z^3D^o:1	0.318595	0.3260611
$3d^3(^2P)4s$	a^1P:1	0.318463	0.3511186
$3d^3(^2D2)4s$	b^1D:2	0.317128	0.3495253
$3d^3(^2H)4s$	a^1H:1	0.311787	0.3401492
$3d^23F4s4pr^3P^o$	z^3G^o:1	0.304281	0.3144135
$3d^23F4s4p^3P^o$	z^1D^o:1	0.300071	0.2945234
$3d^23F4s4p^3P^o$	z^1F^o:1	0.297123	0.2928456
$3d^23F4s4p^3P^o$	z^1G^o:1	0.276254	0.2723900
$3d^23P4s4p^3P^o$	z^3S^o:1	0.274192	0.2802184
$3d^23P4s4p^3P^o$	z^5S^o:1	0.272536	0.2763108
$3d^23F4s4p^1P^*$	y^3F^o:2	0.271033	0.3002414
$3d^3(^4F)4p$	y^3D^{o*}:2	0.270577	0.3057027
$3d^21D4s4p^3P^o$	$^3P^{o*}$:1	0.269075	0.2783897
$3d^23P4s4p^3P^o$	y^5D^o:2	0.266206	0.2835034
$3d^23P4s4p^3P^o$	$^3D^{o*}$:3	0.267607	0.2498264
$3d^3(^4F)4p$	y^5G^o:2	0.257743	0.3099667
$3d^21D4s4p^3P^o$	x^3F^o:3	0.255899	0.2626903
$3d^21D4s4p^3P^o$	x^3D^o:4	0.251290	0.2327731
$3d^23F4s4p^1P^o$	y^3G^o:2	0.249417	0.2822516
$3d^23P4s4p^3P^o$	z^5P^o:1	0.248011	0.2451276
$3d^21D4s4p^1P^o$	y^1D^o:2	0.246982	0.2658016
$3d^3(^4F)4p$	y^5F^o:2	0.239143	0.2837225
$3d^4$	a^5D:1	0.238103	0.2702386
$3d^23F4s4p^1P^o$	w^3D^{o*}:5	0.230385	0.2175197
$3d^3(^2F)4s$	a^1F:1	0.229566	0.2597474
$3d^3(^2F)4p$	x^5D^{o*}:3	0.228262	0.2458402
$3d^21G4s4p^3P^*$	x^3G^o:3	0.228054	0.2354965
$3d^23P4s4p^3P^o$	v^3D^o:6	0.217007	0.1738592
$3d^3(^4F)4p$	w^3G^o:4	0.214093	0.2166774
$3d^23P4s4p^3P^o$	y^3P^o:2	0.211818	0.2359998
$3d^21G4s4p^3P^o$	z^3H^o:1	0.210319	0.2302027
$3d^21D4s4p^1P^o$	y^1F^o:2	0.201868	0.2255881
$3d^3(^4P)4p$	x^3P^o:3	0.199632	0.2036524
$3d^3(^4F)4p$	w^3F^o:4	0.194346	0.1999137
$3d^21D4s4p^1P^o$	z^1P^o:1	0.194551	0.2090194
$3d^21G4s4p^3P^o$	v^3F^o:5	0.190462	0.1835448
$3d^42$	d^3P:4	0.187532	0.1865970
$3d^34d$	^1D:3	0.186932	0.1998364
$3d^3(^2G)4p$	z^1H^o:1	0.185078	0.2166693
$3d^23P4s4p^3P^o$	y^1P^o:2	0.182828	0.1801664
$3d^32P4p$	x^1D^o:3	0.182026	0.1788081
$3d^42$	^3F:4	0.180603	0.1855929
$3d^4$	^3H:2	0.178587	0.1906706

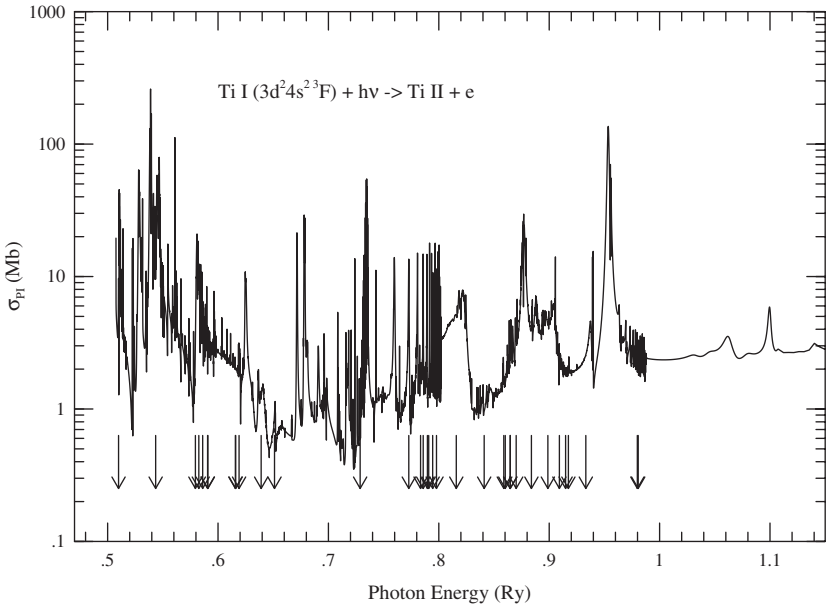

Fig. 1. Photoionization cross sections σ_{PI} of the ground state $3d^2\ 4s^2(^3F)$ of Ti I: the arrows point various core excitations.

NIST table, Similarly $3d^32P4p(u^3D^o)$ differs from $3d^23P4s4p(^1P^o)$, $3d^3(^4P)4p(t^3D^o)$ from $3d^3(^2P)4p(^3D^o)$, and $3d^32D4p(w^1D^o)$ from $3d^32P4p(^1D^o)$, However, these differences do not invalidate the identifications because a mixed state can have different leading percentage from different calculations. Hence the identifications are correct with respect to the method used.

The calculated energies are compared with observed states in Table 2. Very good agreement is found between the calculated and measured values for the ground and many excited states. However, some large differences are also noted. The largest one being 13% for $3d^3(^4F)4sa^5F$ state. The optimization for three states computed by Miecznik and Greene (1996) agree better with experimental values than the present values. For example, they obtain 0.3192, 0.3043, 0.2397 Ry for the three states $3d^23F4s4p^3P^oz^3D^o$, $3d^23F4s4pr^3P^oz^3G^o$, $3d^3(^4F)4py^5F^o$ respectively compared to experimental values of 0.3186, 0.3043, 0.2837 Ry and present values of 0.32606, 0.31441, 0.2397 Ry.

4.2. Photoionization cross sections

Photoionization cross section (σ_{PI}) are presented for all 908 bound states. Currently only limited cross sections for Ti I are available. Illustrative features of photoionization cross sections are described below.

Photoionization of the ground state, $3d^2\ 4s^2(^3F)$ of Ti I is presented in Fig. 1. It shows features, unlike most other ions where the photoionization cross section falls with smooth background, extensive resonances with nonsmooth background. These features indicate significant photoabsorption by the ground state of Ti in the low energy region. This will cause increased opacity in the outer layers of cool stars. To each excited target or core state, C_N there belongs a Rydberg series of autoionizing state, $C_N vl$ where v is the effective quantum number and l is the orbital angular momentum of the outer electron, and C_N is an excited core state, such as, $3d^3(^3F)$ state. However, the background and resonances can be enhanced when the core excitations couple to the state of the $(N+1)$-electron system. All core excitations considered in the calculations are either quartets or doublets and hence couple to the triplet ground state of Ti I (see Table 1) and contribute to formation of features.

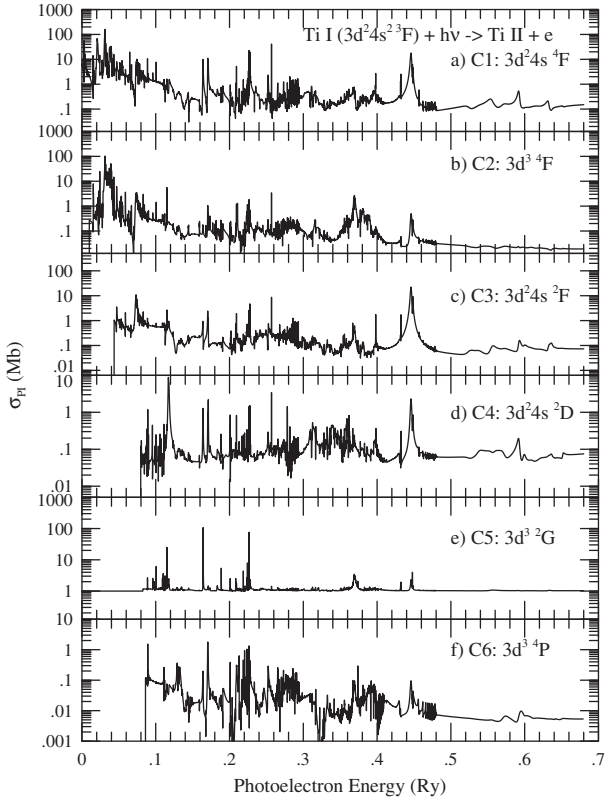

Fig. 2. Partial photoionization cross sections σ_{PI} of the ground state $3d^2\ 4s^2(^3F)$ of Ti I leaving the core Ti II in various states (CN).

Contributions of various channels can be seen from partial cross sections. Fig. 2 presents partial photoionization cross sections of the first six channels where the ionized ground ^3F state of Ti is left at various core states, C_2, C_3, C_4, etc. Each partial cross section, particularly the lower ones, is contributing significantly to the total cross sections. The magnitude of scale in Fig. 2 shows that the first

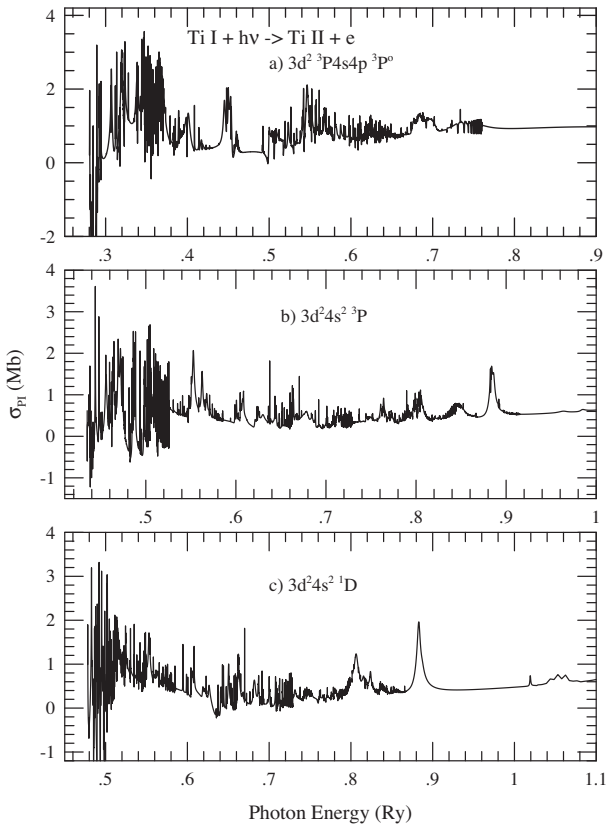

Fig. 3. Photoionization cross sections σ_{PI} of low-lying excited states (a) $3d^2\,^3P4s4p(^3P^o)$, (b) $3d^24s^2(^3P)$, (c) $3d^24s^2(^1D)$. Resonant features in the low energy region will cause photoabsorption and hence increased opacity in the low temperature region.

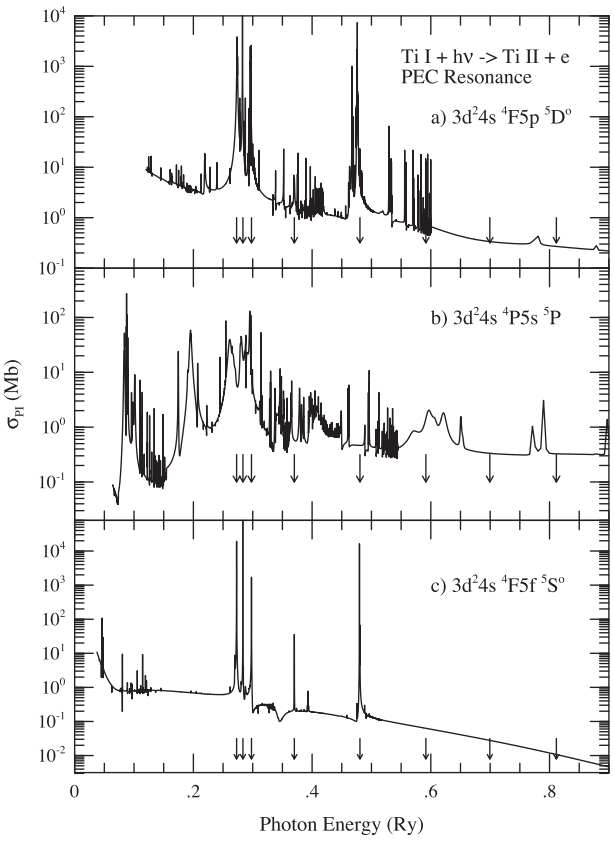

Fig. 4. Photoionization cross sections σ_{PI} of excited states, (a) $3d^24s(^4F)5p(^5D^o)$, (b) $3d^24s(^4P)5s(^5P)$, (c) $3d^24s(^4F)4f(^5S^o)$ of Ti I. Prominent Seaton resonances due to core excitation to various dipole allowed states are indicated by the arrows.

two partial cross sections corresponding to leaving the core at the ground $C_1 : 3d^24s(^4F)$ and excited $C_2 2:3d^3(^F)$ states, which lie very close to each other within 0.01 Ry, contribute the most. The next dominant contributor is $C_5 = 3d^3(^2G)$ which has less features, but relatively stronger background.

Dominant resonant features in the low energy region of photoionization cross sections can also be seen in low lying excited states. Fig. 3 illustrates such features in σ_{PI} of Ti I for the low lying excited states, (a) $3d^2\,^3P4s4p(^3P^o)$, (b) $3d^24s^2(^3P)$, (c) $3d^24s^2(^1D)$ These states can form easily at low temperature and cause enhanced photoabsorption. The resonant structure form will affect quantities in the low temperature plasmas, such as, photoionization rate Γ of an ion X^{i+}. Γ is given by,

$$\Gamma(s^{-1}) = 4\pi \int_{E_o}^{E_{max}} F(E)\sigma_E dE, \qquad (8)$$

where σ_E is the total photoionization cross section in cm^2, $F(E)$ is the photoionizing radiation field, and E_o is the ionization potential of X^{i+}.

The other distinct resonant feature typically seen in photoionization of excited states with single valence electron is the presence of relatively wider Seaton resonances. They are embedded in narrow Rydberg resonances and form due to photo-excitation-of-core (PEC) (Yu and Seaton, 1987). Fig. 4 presents σ_{PI} of three excited levels, (a) $3d^24s(^4F)5p(^5D^o)$, (b) $3d^24s(^4P)5s(^5P)$, and (c) $3d^24s(^4F)4f(^5S^o)$ of Ti I which illustrate Seaton resonances. In the figure, positions of these resonances are pointed out by arrows at various energy positions, The interference between a Seaton resonance and Rydberg series of resonances can enhance the background considerably, as seen in Fig. 4(a) and (b).

These resonances are manifested as the core ground state goes through electric dipole transitions at the corresponding photon energies while the outer electron remains a 'spectator' in a doubly-excited resonant state. The state decays via autoionization into the ground level of the core as the photoelectron ejects out. The core ground level $3d^24s(^4F)$ can be excited to $3d^2(^4F)4p(^4G^o)$ state at 0.273 Ry and form Seaton resonance at $^4G^o_1$ threshold, as seen in σ_{PI} of the excited states in Fig. 4. These resonances appear at photon energies that match the core excitation energies for dipole allowed transitions, regardless of the state of the ion. There may be slight variations in positions due to interferences of resonances and one or more resonances may be less distinct or one may not show up in σ_{PI}. Seaton resonances, in general, become more distinct in photoionization of higher excited levels.

McLaughlin and Duquette (1992) measured averaged σ_{PI} in a small energy range of excited $3d^24s4p(^3P_2)$ level of Ti I using pulsed-laser excitation and ionization. However they found considerable structure in cross sections, presented in Fig. 4(b) of their paper, and explained that the excited state rapidly undergoes radiative decay on to the ground or low lying states. The present results verify their findings of resonant structures and identify that the observed features are largely from two low lying states, $3d^24s^2(^3F)$ and $3d^24s^2(^1D)$, of Ti I. Fig. 5 presents σ_{PI} of these two states in the energy region studied in the experiment and compare with the measured spectrum. They were able to measure parts, not the whole energy range, of the spectrum. The location of the structures in the measured spectrum in the top panel of Fig. 5 can be identified from the theoretical structures in the lower panel.

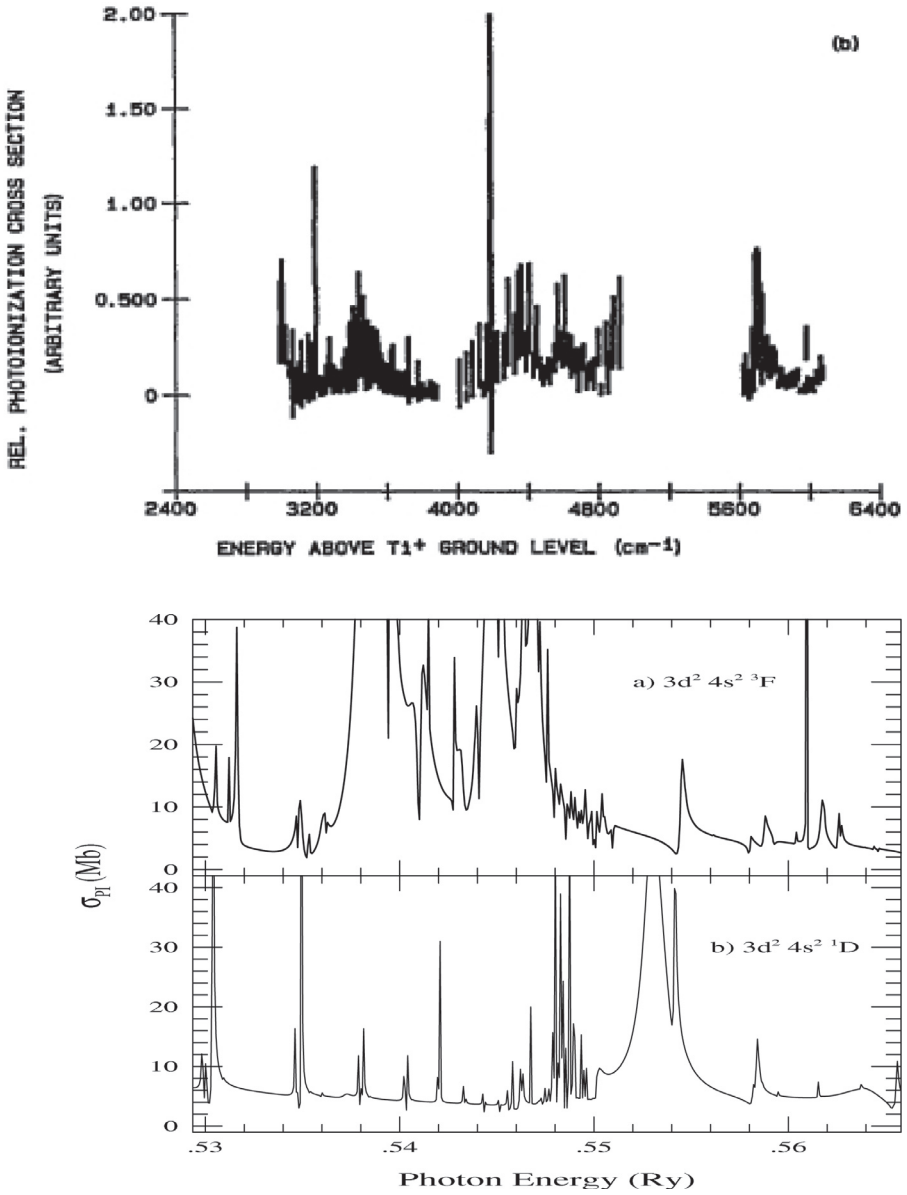

Fig. 5. Photoionization cross sections σ_{PI} of two states, (a) $3d^2 4s^2 (^3F)$ and (b) $3d^2 4s^2 (^1D)$ of Ti I are compared with the measured spectrum (top subplot) by McLaughlin and Duquette McLaughlin and Duquette, 1992. Theoretical energy range corresponds to that of the measured cross sections. The measured resonant features can be identified in σ_{PI} of ^3F and ^1D states.

The present LS coupling calculations show extensive resonances due to strong couplings with the core states. Inclusion of relativistic effects is expected to produce additional resonances through couplings of fine structure levels. The computations will be extensive due to two reasons. The number of energy levels of will increase to a several thousands. The number of core levels will also increase by a few times. The current set of 36 LS states in the wave function expansion corresponds to 90 fine structure levels. Accordingly the number of series of resonances due to autoionizing states will also increase. To delineate these narrow resonances, much finer energy mesh will be needed. The present results will provide a guide to this calculations for higher accuracy.

5. Conclusion

An extensive set of photoiozation cross sections for a large number of excited states, 908 in total, have been presented, These should provide a more complete modeling of astrophysical and laboratory applications. The resonances, particularly in the low energy region, have been delineated with fine energy mesh. Important resonances are found at low energy region which should provide better understandings of Ti lines found in various cool stars. The results should have significant contributions in photoionization and recombination rates at temperatures where Ti I exist in plasmas in various cool stars and in determination of abundance of Ti in these objects. The present work finds enhanced background cross sections of excited levels of by the Seaton resonances formed during dipole allowed core excitations. The present cross sections are expected to be of accuracy of about 20–30% based on (i) large number of core excitations, (ii) higher resolution for resonances, (ii) consideration of large number configurations, and good agreement of present energies and photoionization cross sections with the available published values.

All photoionization data are available electronically from online NORAD-Atomic-Data page at (NaharOSURadiativeAtomicData) website: http:/www.astronomy.ohio-state.edu/nahar/nahar_radiativeatomicdata.

Acknowledgments

This work was supported partially by NSF AST-1312441 and AST-1109088. The computational work was carried out at the Ohio Supercomputer Center (OSC) in Columbus Ohio.

References

Berrington, K.A., Burke, P.G., Butler, K., Seaton, M.J., Storey, P.J., Taylor, K.T., Yu, Y., 1987. J. Phys. B 20, 6379.
Burke, P.G., Robb, W.D., 1975. Adv. At. Mol. Phys. 11, 143.
Eissner, W., Jones, M., Nussbaumer, H., 1974. Comput. Phys. Commun. 8, 270.
Hummer, D.G., Berrington, K.A., Eissner, W., Pradhan, A.K., Saraph, H., Tully, J.A., 1993. Astron. Astrophys. 279, 298.
Keenan, P.C., 1982. Astron. Soc. Pacific 94, 299.
McLaughlin, K.W., Duquette, D.W., 1992. J. Opt. Soc. Am. B 9, 1953.
Miecznik, G., Greene, C.H., 1996. J. Opt. Soc. Am. B 13, 244.
Nahar, S.N., 2006. A&A 448, 779.
Nahar, S.N., Pradhan, A.K., 1991. Phys. Rev. A 44, 2935.
Nahar, S.N., Eissner, W., Chen, G.X., Pradhan, A.K., 2003. A&A 408, 789.
Page, R.H., Gudeman, C.S., 1990. J. Opt. Soc. Am. B 7, 1761.
Pradhan, A.K., Nahar, S.N., 2011. Atomic Astrophysics and Spectroscopy. Cambridge University Press.
Saloman, E.B., 2012. J. Phys. Chem. Ref. Data 41, 013101.
Seaton, M.J., 1987. J. Phys. B 20, 6363.
Sohl, J.E., Zhu, Y., Knight, R.D., 1990. J. Opt. Soc. Am. B 7, 9.
The Opacity Project Team. The Opacity Project, vol. 1, 1995, vol. 2, 1996, Institute of Physics Publishing.
Valenti, J.A., Piskunov, N., Johns-Krull, C.M., 1998. ApJ 498, 851.
Wood, P., Kotachery, D., van Winckel, H., 2013. MNRAS 435, 355.
Yu, Y., Seaton, M.J., 1987. J. Phys. B 20, 6409.
<http://physics.nist.gov/PhysRefData/ASD/levels_form.html>.